Simulate Time-integrated Coarse-grained Molecular Dynamics with Geometric Machine Learning

Xiang Fu[1*†], Tian Xie[1†], Nathan J. Rebello[2], Bradley D. Olsen[2] and Tommi Jaakkola[1*]

[1*]CSAIL, MIT, Cambridge, 02139, MA, United States.
[2]Department of Chemical Engineering, MIT, Cambridge, 02139, MA, United States.

*Corresponding author(s). E-mail(s): xiangfu@csail.mit.edu; tommi@csail.mit.edu;
Contributing authors: txie@csail.mit.edu; nrebello@mit.edu; bdolsen@mit.edu;
†Equal Contribution.

Abstract

Molecular dynamics (MD) simulation is the workhorse of various scientific domains but is limited by high computational cost. Learning-based force fields have made major progress in accelerating ab-initio MD simulation but are still not fast enough for many real-world applications that require long-time MD simulation. In this paper, we adopt a different machine learning approach where we coarse-grain a physical system using graph clustering, and model the system evolution with a very large time-integration step using graph neural networks. Despite only trained with short MD trajectory data, our learned simulator can generalize to unseen novel systems and simulate for much longer than the training trajectories. Properties requiring 10-100 ns level long-time dynamics can be accurately recovered at several-orders-of-magnitude higher speed than classical force fields. We demonstrate the effectiveness of our method on two realistic complex systems: (1) single-chain coarse-grained polymers in implicit solvent; (2) multi-component Li-ion polymer electrolyte systems.

Molecular dynamics (MD) simulation techniques have become an essential computational tool in many natural science disciplines, making massive progress across various atomic systems like inorganic materials, polymers, proteins, with applications including optimizing Li-ion transport in polymer electrolytes for batteries [1–3], understanding protein folding dynamics [4, 5], etc. A major limitation of MD simulation is its high computational cost, especially for complex systems like polymers and proteins. Such simulations typically involve tens of thousands of atoms and can reach nanosecond- to microsecond level to properly sample the free energy landscape. A single simulation can often take weeks or even months, making large-scale screening extremely expensive or even infeasible.

Machine learning (ML) force fields [6–11] have made important progress towards accelerating MD simulations, achieving ab-initio level accuracy with significantly lower computational costs [12–15] and generalizing to new atomic systems [16, 17]. However, learning-based force fields alone are still not enough to simulate complex atomic systems due to two major limitations: 1) the time integration step for the force fields is still at the femtosecond level, which means that millions of steps are needed to achieve a nano-second level simulation; 2) learning-based force fields are susceptible to become unstable after long-time simulation [9, 18]. Coarse-grained (CG) models [19–21]

Tian Xie's current affiliation: Microsoft Research, Cambridge CB1 2FB, United Kingdom

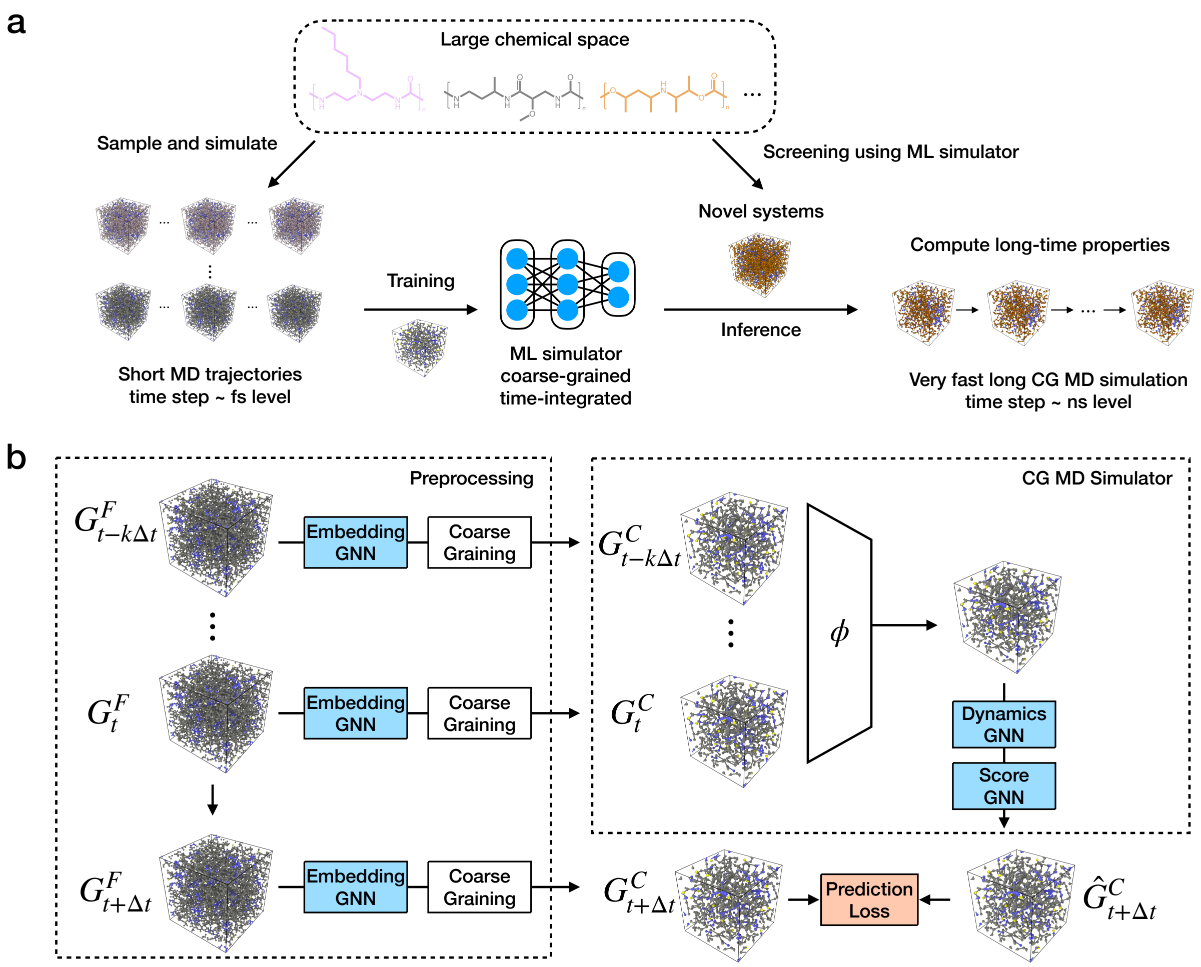

Fig. 1 (a) To reduce the computational cost for estimating long-time properties of complex systems, our learned simulator is trained over short ground truth MD trajectories of sampled systems. Being several orders of magnitude more efficient, the learned simulator is used to simulate long time-integrated CG MD trajectories for novel systems, starting from a very short history as the initial state. (b) Learning time-integrated CG MD with multi-scale graph neural networks. Trainable modules are colored in blue. The loss term is colored in red. The preprocessing steps embed and coarse-grain an MD system to a coarse-level graph. The CG MD simulator featurize historical information using the featurizer ϕ, after which the Dynamics GNN predicts the next-step positions. A Score GNN can be optionally applied to further refine the predicted positions.

tackles these challenges by reducing system complexity and increasing the time-integration steps. However, CG schemes are usually limited to specific systems [22] and still require short time integration. Enhanced sampling methods offer a different approach [23–25] by modifying the potential energy surfaces to enable faster sampling of transition between metastable states. They often require identifying collective variables (CVs) in advance. ML has been used to augment these methods [26] in free energy surface approximation [27], obtaining latent CV [28], etc. But it is still difficult to determine the CVs, or apply enhanced sampling methods for complex systems [25]. Moreover, there is no explicit notion of "time" in enhanced sampling, making them infeasible for the extraction of dynamical properties [29, 30]. In addition, ML generative modeling approaches [31, 32] have enabled fast sampling of equilibrium states across phases for systems but are unable to produce realistic MD trajectories to study the dynamical behavior of atomic systems or generalize across different molecular systems.

We present a different approach by learning a graph neural network (GNN) [33–36] based simulator that reduces computation cost from both temporal and spatial perspectives: (1) instead of running the simulation at a time step of 1-10 fs which is typical for MD and coarse-grained MD; the simulator can run MD at a significantly larger time step at the ns-level by learning time-integrated acceleration from data; (2) instead of running the simulation at a full-atom scale, the simulator run MD at a coarse-grained level. Our goal is to learn such a time-integrated, coarse-grained MD simulator from trajectory data, where important properties that we aim to extract from the original trajectories can be efficiently obtained. Different from previous ML force field or coarse-grained modeling approaches, our method lifts the limitation of short time-integration time, as we directly predict dynamics rather than forces. Unlike enhanced sampling methods, our model does not require knowing CVs and is trained to recover the true dynamics, thus able to recover accurate static and dynamical properties. Going beyond existing ML generative models, our learned simulator enables the extraction of dynamical properties and can generalize across various atomistic compositions. The unparalleled speed of our method enables us to solve and generalize over very challenging long-time simulation tasks for very complex systems that are infeasible for existing approaches.

A high degree of coarse-graining and very long time integration greatly accelerate the simulation, but also make the dynamics non-Markovian and uncertain [37]. We introduce several technical modifications such as multi-scale modeling, incorporation of historical information, and stochastic prediction to overcome these challenges. The well-known instability issue of long-time learned simulation becomes more salient under our very challenging simulation setup. We adopt a novel score-based [38] refinement module, which iteratively refines a potentially erroneous structure to a physical configuration. Our experiments demonstrate the effectiveness of the score-based refinement module in resolving simulation instability.

We demonstrate the effectiveness of our approach by simulating two realistic complex systems of high practical significance: (1) single-chain coarse-grained polymers and (2) multi-component Li-ion polymer batteries. We aim to learn from a limited amount of short training MD trajectories, and generate significantly longer MD simulations for novel systems to obtain long-time dynamical properties that can only be reliably extracted from long simulations. While our task is very challenging, our model is shown to be stable, generalizable, accurate, and efficient. Given a short ground truth state history as the starting point, trajectories of horizons 10-100x longer than the training trajectories can be simulated for new systems, remaining stable and realistic all the time. Long-time properties computed from long simulations of our model accurately recover the results from expensive long MD simulations. Our model dramatically reduces the time and compute requirement of estimation problems with long simulation, achieving several-orders-of-magnitude speedup compared to classical force fields.

Results

As shown in Fig. 1 (a), we aim to learn a coarse-grained, time-integrated simulator from a list of short MD trajectories of atomic structures sampled from a given chemical space. Since the short MD trajectories cover most atomic structures and dynamics, we hope the simulator can generalize to novel atomic systems sampled from the same chemical space and run significantly longer simulations than the training trajectories. We can extract long-time properties from the longer trajectories which are hard to estimate with the short training trajectories.

The learned simulator predicts single-step time-integrated CG dynamics at time $t+\Delta t$ given the current CG state and k historical CG states at $t, t-\Delta t, \ldots, t-k\Delta t$. Here Δt is the time-integration step, which is significantly longer than that used in traditional MD simulation. Given ground truth trajectories at atomic resolution, we adopt a 3-step multi-scale modeling approach:

1. *Embedding*: learning atom embeddings at **fine level** using an Embedding GNN GN_E;
2. *Coarse-graining*: coarse-graining the system using graph clustering, and constructing CG-bead embedding from atom embedding learned at step 1;
3. *Dynamics* (and *Refinement*): learning time-integrated acceleration at **coarse level** using a Dynamics GNN GN_D. A Score GNN GN_S is optionally learned to further refine the predicted structure.

All neural network modules in the pipeline are trained end-to-end to model single-step CG dynamics. At test time, step 1 and 2 are the preprocessing steps, that we apply only once to a short history of k-step initialization states. The preprocessing outputs a k-step coarse-level state history as the initial input for the CG MD simulator. After preprocessing, step 3 is iteratively executed to simulate long MD trajectories. The generalizability of our model allows long-time properties of novel systems to be efficiently computed with significantly reduced computational cost. Fig. 1 (b) provides an overview of our learned simulator.

Construct CG-bead embedding and CG graph. Given a ground truth MD simulation trajectory as a time series of fine-level graphs $\{G_t^F\}$, step 1 and 2 of the model pipeline construct CG-bead embeddings and coarse-level graphs $\{G_t^C\}$. At the fine-level, each node in the graph represents an atom, and each edge represents a chemical bond. In step 1, the Embedding GNN GN_E constructs time-invariant atom embeddings $\mathrm{GN}_E(G^F)$ from the static fine-level graph G^F, which describes all persistent features (e.g., atom and bond types) of the MD system. Then in step 2, coarse-level graphs $\{G_t^C\}$ are obtained through the CG model. The CG model assigns atoms to different atom groups, and then maps each group to a CG-bead.

We make atom group assignments using a graph clustering algorithm (METIS [39]). The clustering process partitions the fine-level graph into roughly equal atom groups of a specified size, while minimizing the number of bonds with two endpoints in different groups. By changing the atom group size, we can apply the graph clustering algorithm and find the best resolution for modeling a given system. We include more details and illustrations of the coarse-graining process in the Supplementary Information. Once constructed, the CG-bead embeddings remain unchanged in step 3, when CG MD is simulated. This modeling strategy is similar to traditional CG models [40], where the CG-beads are constructed a priori and do not change throughout the CG MD simulation.

Learning time-integrated CG dynamics. At step 3, the Dynamics GNN GN_D inputs a featurized coarse graph $\phi(\{G_{t-i\Delta t}^C\}_{i=0}^k)$, with the featurizer ϕ processing the coarse-level graphs $G_{t-k\Delta t}^C, \dots, G_t^C$ of the current step and k historical steps. The output $\mathrm{GN}_D(\phi(\{G_{t-i\Delta t}^C\}_{i=0}^k))$ is a 3-dimensional Gaussian with mean $\boldsymbol{\mu}_{m,t}$ and variance $\boldsymbol{\sigma}_{m,t}^2$ for each CG-bead m, which denotes a distribution of time-integrated acceleration for the bead. The training loss L_{dyn} for CG dynamics learning is the negative log-likelihood of the ground truth time-integrated acceleration. At inference time, the predicted acceleration is integrated over current positions/velocities using an Euler integrator to obtain the next-step positions for the predicted CG state $\hat{G}_{t+\Delta t}^C$. Due to (1) randomness in MD (e.g., implicit solvent), (2) CG modeling, and (3) long time-integration, including historical information and stochastic prediction are both critical in learning the dynamics. We further explain these modeling choices in Discussion and Supplementary Information.

Learning to refine CG MD predictions. One common challenge for learning-based simulators is that the system can often go to a state that is outside the training distribution after long simulation [9, 18]. Then, the learned dynamics is prone to make prediction errors, which may lead the simulation to unphysical states, and eventually, the system would collapse. In our model, we resolve this issue by using a *Refinement* step. A Score GNN GN_S that rectifies incorrect 3D configurations and stabilize the MD simulation is added, and all modules are still trained end-to-end. With the Score GNN, each forward dynamics step follows a predict-then-refine fashion; with GN_D first make the (potentially noisy) next-step prediction $\tilde{G}_{t+\Delta t}^C$, which GN_S would refine to the final prediction: $\mathrm{GN}_S(\tilde{G}_{t+\Delta t}^C) = \hat{G}_{t+\Delta t}^C$.

Single-chain coarse-grained polymers. We first demonstrate our model's capability to simulate MD of single-chain CG polymers in implicit solvent. Polymer functionality is decided by macromolecular properties at a large time/length-scale, and (CG) MD simulation has been widely used to obtain important properties in practical material design efforts [41–43]. We adopt the polymers introduced in [43], where all polymers are composed of four types of beads and ten types of constitutional units (CUs). We train on regular copolymers with an exact repeat pattern of four CUs (class-I), and test on random polymers constructed from four CUs (class-II). This distribution shift (Fig. 2 (a)) poses great

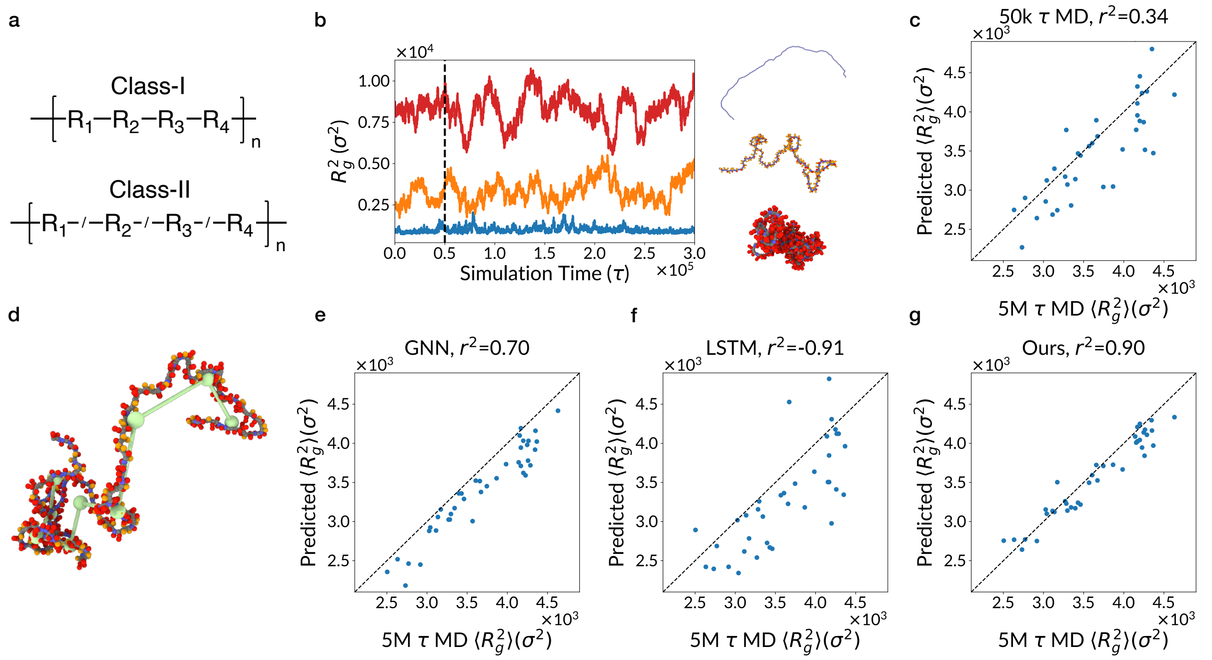

Fig. 2 (a) Class-I polymers are used for training, while class-II polymers are used for testing. The structure variation requires the model to learn generalizable dynamics. (b) R_g^2 for the three training polymers with smallest, median, and largest $\langle R_g^2\rangle$, over a 300k τ period. Our training trajectories are 50k τ long (black dashed line), while we use 5M τ long trajectories for evaluation. (c) Short ground truth MD of training trajectory length gives high-variance, poor estimation of $\langle R_g^2\rangle$. (d) Example polymer before and after coarse-graining. The green beads and bonds represent the CG structure. (e, f, g) $\langle R_g^2\rangle$ estimation performance of the supervised learning baselines using (e) GNN, (f) LSTM, and (g) our learned simulator.

challenge on generalization. All polymers are randomly sampled and simulated under LJ units with a time-integration of 0.01 τ. Each polymer on average contains 889.5 beads.

Radius of gyration (R_g^2) is a property practically related to the rheological behavior of polymers in solution and polymer compactness that are useful for polymer design [43–45]. Reliable estimation of R_g^2 statistics requires sampling with long enough MD simulation, while short simulation results in high variance and significant error. Fig. 2 (b) shows how R_g^2 rapidly changes with time. Fig. 2 (c) shows the poor performance of using 50k τ short MD trajectories to estimate $\langle R_g^2\rangle$ computed from 5M τ trajectories.

Accurate polymer R_g^2 estimation using learned simulation. We train our model on 100 short class-I MD trajectories (with 10 trajectories for validation) of 50k τ, and evaluate on 40 testing class-II polymers using trajectories of 5M τ (100x longer). We take CG modeling one step further by grouping every 100 beads into a super CG-bead (Fig. 2 (d)). For accurate R_g^2 prediction, we use another neural network that inputs the coarse-level latent graph representation to fit the residual of R_g^2 computed from the coarse-level states (as opposed to the fine-level states). A time integration of $\Delta t = 5\tau$ is used, so every step of the learned simulator models the integrated dynamics of 500 steps from training trajectories. At test time, we use the learned simulator to generate 5M τ trajectories and compute properties. With the system significantly simplified by coarse-graining, long and stable simulation can be achieved without using a Score GNN for refinement.

We compare our model to two supervised-learning (SL) baseline models, one based on GNN and another based on long short-term memory [46] (LSTM) networks. SL models input the polymer graph structure and directly predict the mean and variance of R_g^2 without learning the dynamics (details in Method). Fig. 2 (e) and (f) shows the prediction of $\langle R_g^2\rangle$ of two baseline SL models, while Fig. 2 (g) shows the performance of our learned simulator. Table 1 summarizes more performance metrics. Our method significantly outperforms the

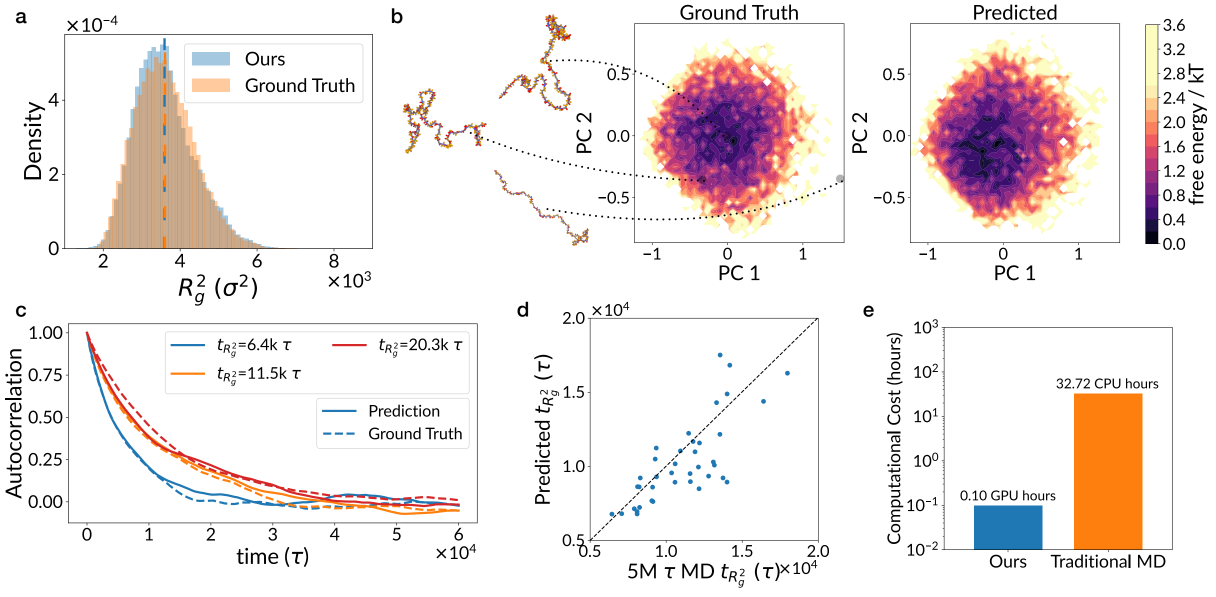

Fig. 3 (a) R_g^2 distribution computed from our learned simulation matches the ground truth. The vertical dashed lines annotate the mean of the distribution. (b) Two-dimensional free energy surface produced with PCA, with representative states with low/high free energy visualized. (c) The autocorrelation function of R_g^2, for the three polymers with the smallest, median, and the largest relaxation time. (d) Prediction performance of our model on the R_g^2 relaxation time. (e) Computational cost comparison of our learned simulation vs. traditional MD. The y-axis is at log-scale.

baseline models and estimation from short 50k τ MD trajectories (Fig. 2 (c)) in all metrics. In particular, the earth mover's distance (EMD) is a measure of distribution discrepancy. A lower EMD indicates a better match between the predicted R_g^2 distribution and the ground truth. With only short trajectories for training, The SL models can only fit the high-variance statistics and produce poor results. Our testing polymers come from a different distribution from training. We, therefore, observe a systematic underestimation for the SL baseline. On the other hand, our learned simulator learns dynamics that generalize to a different class of polymers and longer time horizon, and produces accurate long-time property estimation. We also experiment with existing learned simulator model [35], but find it quickly diverges under the long-time simulation task setup.

Recovery of long-time distributional and dynamical properties. For the testing polymer with median $\langle R_g^2 \rangle$, Fig. 3 (a) demonstrates that the R_g^2 distribution produced by our model matches very well with the ground truth, confirming the low EMD achieved. We also visualize 2-dimensional free energy surfaces of the ground truth simulation and our learned simulation. The surfaces are produced by fitting a projection map using principal component analysis (PCA) over the ground truth CG-bead pairwise distances and applying the same projection to the model-predicted data. Finally, we show our learned simulator can capture the long-time dynamics in the autocorrelation function (ACF) of R_g^2. Fig. 3 (c) shows the ACF computed from our learned simulation matches the ground truth. We obtain the relaxation time $t_{R_g^2}$ from the ACFs (details in Method) and achieve a r^2 of 0.48 (Fig. 3 (d)) using learned simulation. The relaxation time is a long-time dynamical property that is significantly more challenging to estimate than $\langle R_g^2 \rangle$. It can

Table 1 Performance for predicting R_g^2 statistics. r^2 and MAE are computed for $\langle R_g^2 \rangle$, and EMD is computed for R_g^2 distribution. To evaluate EMD, the SL models output a Gaussian distribution with the predicted mean and variance.

Method	r^2 (↑)	MAE (↓)	EMD (↓)
Short MD, 50k τ	0.34	349	4.10
GNN, SL	0.70	263	2.82
LSTM, SL	-0.91	559	5.82
Ours, 5M τ	**0.90**	**140**	**1.60**

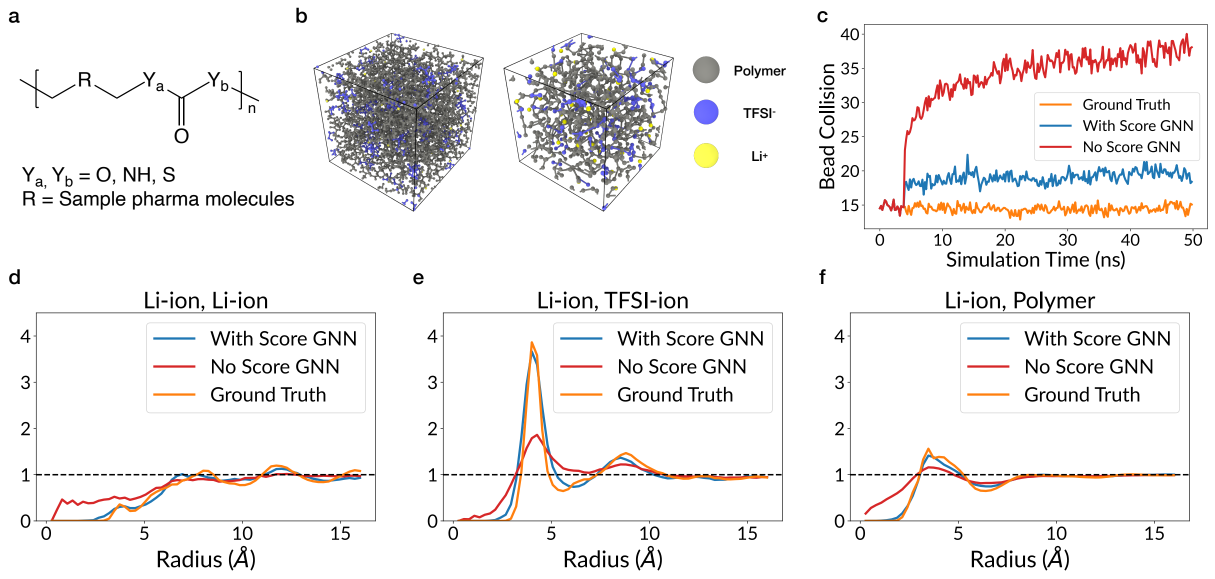

Fig. 4 (a) The chemical space for the polymer in SPEs. (b) Example SPE before and after coarse-graining. (c) Bead collision as a function of simulation time, averaged over the 50 testing SPEs for all methods. (d) RDF of Li-ions, for our model with/without the Score GNN refinement, and the ground truth MD simulation, averaged over a 50-ns trajectory of a selected SPE. (e) RDF of Li-ions and TFSI-ions. (f) RDF of Li-ions and polymer particles.

not be obtained from many independent samples of polymer states and requires simulation much longer than our training trajectories to estimate accurately. Recovery of $t_{R_g^2}$ shows that our model captures realistic dynamics rather than just the distribution of states. Finally, Fig. 3 (e) shows the significant computational cost saving using our learned simulation.

Multi-component Li-ion polymer electrolyte systems. To further demonstrate the effectiveness of our approach, we apply our model to a significantly more complex system – solid polymer electrolytes (SPEs, visualized in Fig. 4 (b)), a type of amorphous material system that is promising in advancing Li-ion battery technology [47]. Atomic-scale MD simulations have been an important tool in SPE studies [1, 3, 48, 49], but are very computationally expensive. Usually containing multiple components with thousands of atoms, the SPE systems are inherently very complex. The challenge also comes from their amorphous nature and the slow convergence of key quantities (Fig. 5 (b)), requiring long MD simulations on the order of 10 to 100 ns to estimate.

We adopt the SPEs introduced in [49], where each MD trajectory contains a system with a distinct type of polymer as illustrated in Fig. 4 (a) mixed with lithium bis-trifluoromethyl sulfonimide (LiTFSI) under periodic boundary conditions. We train on 530 short MD trajectories of 5 ns (with 30 trajectories for validation), and evaluate on 50 novel SPE trajectories of 50-ns long. On average each SPE system contains 6025 atoms. Our CG model groups every 7 bonded atoms into a CG-bead (Fig. 4 (b)). We use a time-integration of $\Delta t = 0.2$ ns, making each step of the learned simulator equivalent to 10^5 steps in training trajectories. We include blation studies on the hyperparameters in the Supplementary Information.

Stability of learned simulation and Score GNN refinement. Unlike the single-chain polymers, learned simulation for the more complex SPEs suffers from the out-of-distribution prediction problem, which we resolve with the Score GNN refinement step. As a measure of stability, we consider a "bead collision" happen when two beads have a distance below 1.0 Å. A large number of bead collisions indicates the system is unphysical. Fig. 4 (c) demonstrates the number of bead collisions as a function of simulation time, averaged over all 50 test SPEs.

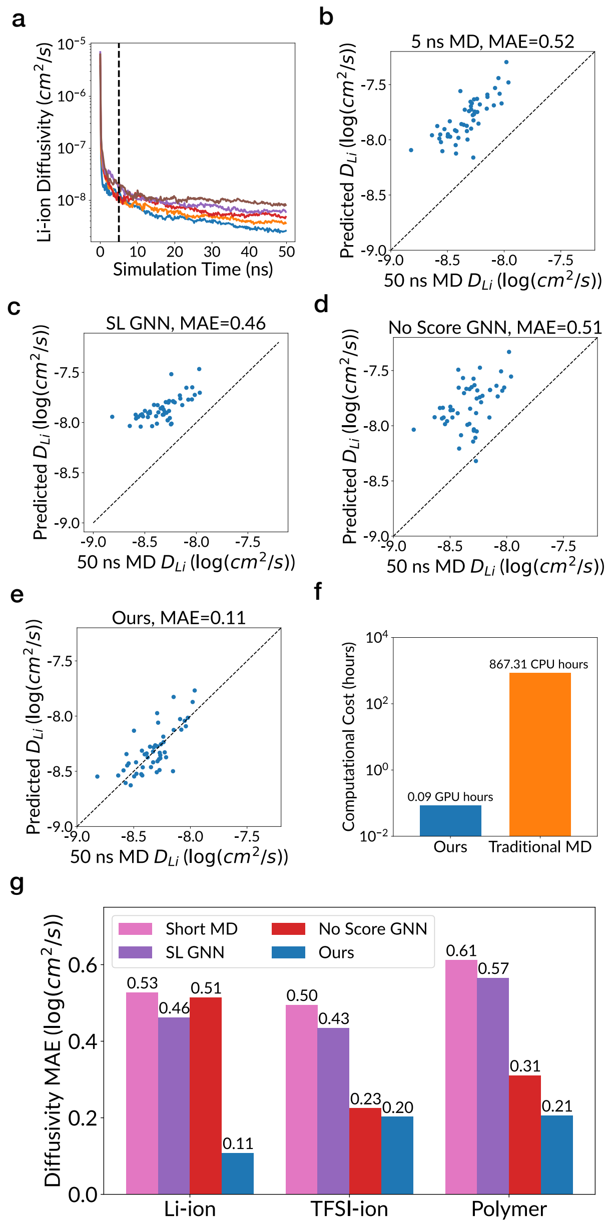

Fig. 5 (a) Slow convergence of Li-ion diffusivity. Estimating this long-time property with only 5 ns training trajectories (black dashed line) is very challenging. (b) 5-ns MD gives a poor estimation of Li-ion diffusivity. (c, d, e) Performance of SL GNN model, learned simulator without Score GNN refinement, and our full model in Li-ion diffusivity prediction. Only our full model is able to predict long-time property from short training trajectories only. (f) Computational cost of our learned simulator vs. traditional MD. The y-axis is at log-scale. (g) Performance of all models in predicting diffusivity of Li-ion, TFSI-ion, and polymer particles.

Simulation without Score GNN refinement suffers from bead collision, and the system becomes increasingly unphysical as simulation proceeds. The Score GNN refinement significantly reduces collision. The system remains stable and realistic for the entire 50-ns simulation. In Fig. 4 (d), (e), and (f) we plot radial distribution functions (RDFs) averaged over the 50-ns simulation for an example testing SPE over (d) Li-ions; (e) Li-ions and TFSI-ions; and (f) Li-ions and polymer beads. The excessive-high density at a near distance and missed radius peaks confirm the bead collision and instability without Score GNN refinement. With Score GNN refinement, the learned simulation produces RDFs that can recover the overall shape and radius peaks of the ground truth. More RDFs are included in the Supplementary Information.

Estimate long-time ion-transport properties using learned simulation. We next investigate our model's capability in predicting long-time properties of SPEs. One key challenge in simulating the Li-ion transport in SPEs is the slow relaxation process in amorphous polymers. Consequently, estimating the diffusivity of particles like Li-ions requires very long simulation time to sample the dynamics (Fig. 5 (a)). Li-ion Diffusivity (D_{Li}) computed from short MD significantly overestimates the the converged quantity (Fig. 5 (b)). As only 5-ns trajectories are available for training, a strong SL GNN model adopted from [49] that inputs the polymer chemical structure struggles to fix the systematic error (Fig. 5 (c)), even after special treatment against overestimation (details in Method). Without the Score GNN refinement, learned simulation becomes unphysical and overestimates D_{Li} (Fig. 5 (d)).

Our model with Score GNN refinement is able to learn accurate and generalizable dynamics, achieving an MAE of 0.11 for predicting 50-ns D_{Li} (Fig. 5 (e)). One significant aspect of this result is long-time properties are accurately predicted with significantly shorter trajectories for training. This is possible because the forces that govern the interaction between particles are consistent irrespective of simulation length, and our learned simulator is capable of learning the interaction from short trajectories. Fig. 5 (f) compares the computational cost, while Fig. 5 (g) summarizes the diffusivity prediction performance for all particle types. Our learned simulation produces the best result, with a computational cost that is orders-of-magnitude lower than traditional MD.

Discussion

We have developed a machine learning model for simulating time-integrated CG MD that is orders of magnitude faster than traditional MD. The learned CG dynamics is at a lower spatio-temporal resolution, but can be stably simulated for a very long time, while important properties can be accurately extracted. Our simulator is only trained over short training MD trajectories, but can generalize well to simulate much longer trajectories for novel unseen systems. In two challenging and realistic applications, our model significantly outperforms supervised learning baseline methods, as well as directly using short-time MD for property estimation.

Different from previous ML force field methods, our model bypasses force computation, and directly predicts time-integrated acceleration at the CG level, using a very large time-integration step. The spatio-temporal coarse-graining introduces memory effects (i.e., the system becomes non-Markovian) [37] and a high degree of uncertainty. We make several technical innovations to deal with these new challenges: (1) Historical information is used for predicting the next state. Our ablation study shows that historical information plays a very important role in getting better performance. (2) The model predicts stochastic acceleration instead of deterministic forces. A model that makes deterministic prediction fails to capture realistic dynamics. (3) A fine-level Embedding GNN constructs CG-bead types based on local atomic structures to characterize the coarse-level interactions. Model performance significantly drops without the Embedding GNN. (4) A Score GNN refinement step to resolve the long-standing instability problem of long-time learned simulation. Ablation studies in the Supplementary Information systematically demonstrates the influence of these modifications.

Practically, our model can be used for large-scale MD screening of a large chemical space by (1) sample systems from the target chemical space to simulate short trajectories using traditional MD; (2) train our CG MD simulator over the short MD trajectories; (3) use the learned simulator to simulate long MD trajectories for the large chemical space (Fig. 1 (a)). Such screening can be very computationally expensive entirely using traditional MD, especially because of the difficulty in parallelizing long-time simulations. Using our model, one just needs to simulate a set of short trajectories that is easy to parallelize, and long trajectories can be very efficiently generated using the learned simulator.

Some molecular systems obey symmetries in the form of invariance and equivariance. These symmetries can be enforced with special feature representation and model architecture, or learned from data. Our model enforces translational invariance, but does not enforce rotational equivariance. Instead, our model is able to learn this equivariance from data and become "effectively rotationally equivariant" when the equivariance exists (e.g., for the single-chain polymer system). We conduct experiments to apply random rotations at X, Y, and Z axes to input data, and the time-integrated acceleration predicted by our model is accordingly rotated by the same amount. Because many MD systems are not rotationally equivariant (e.g., when an external field such as an electric field is present), we present our model as a general approach that is applicable to diverse systems. When the system is known to have symmetry properties, enforceng them with architectures such as equivariant neural network [50–54] may further improve the data efficiency and generalization capability of our model.

In addition, the spatial coarse-graining and large time-integration simplify the dynamics, as high-frequency detailed dynamics is lost. This dynamics simplification is a two-edged sword: the simplified dynamics can be easier to learn and requires a lower computational cost to simulate, but the lost information may lead to inaccurate dynamics and errors in property estimation. Therefore, the optimal CG modeling is closely tight to the final objective of the MD simulation. The simple graph-clustering CG model used in our method does not offer justification on what information is preserved, and may appear insufficient for more complex systems. CG modeling based on the essential dynamical information, and more sophisticated CG modeling techniques [19, 55–61] is another important future direction in designing more effective CG MD simulation schemes.

Methods

Graph processing with graph neural networks. A graph neural network takes graphs $G = (V, E)$ with node/edge features as inputs and processes a latent graph $G^h = (V^h, E^h)$ with latent node/edge representation through several layers of learned message passing. In this paper we adopt the ENCODER-PROCESSOR-DECODER architecture [35, 36] for all GNNs, which inputs featurized graph and outputs a vector for each node. The ENCODER-PROCESSOR-DECODER model is constructed with three submodules, and a forward pass through the GNN follows three steps: (1) The ENCODER contains a node multi-layer perceptron (MLP) that is independently applied to each node, and an edge MLP that is independently applied to each edge to produce encoded node/edge features. (2) The PROCESSOR is composed of several layers of directed message passing layers. It generates a sequence of updated latent graphs and outputs the final latent graph. The message passing layers allow information to propagate between neighboring nodes/edges. (3) The DECODER is a node-wise MLP that is independently applied to the node features obtained from message passing to produce the outputs of a specified dimensionality. We refer interested readers to [35] for more details on the GNN architecture.

In our implementation, we use 2 hidden layers for all MLPs and 7 message-passing layers for all GNNs. The Embedding GNN GN_E has a hidden size of 64, while the Dynamics and Score GNNs have a hidden size of 128. All activation functions in the neural networks are rectified linear units (ReLU). We train the model for 2 million steps. The network is optimized with an Adam optimizer with an initial learning rate of 2×10^{-4}, exponentially decayed to 2×10^{-5} over the 2 million training steps. All models are trained and used for producing long simulations over a single RTX 2080 Ti GPU.

Representing MD trajectories as time series of graphs. A ground truth MD simulation trajectory is represented as a time series of fine-level graphs $\{G_t^F\}$. The fine-level graph G_t^F represents the MD state at time step t, and is defined as a tuple of nodes and edges $G_t^F = (V_t^F, E^F)$. Each node $\boldsymbol{v}_{i,t}^F \in V_t^F$ represents an atom [1], and each edge $\boldsymbol{e}_{i,j}^F \in E^F$ represents a chemical bond between the particles $\boldsymbol{v}_i^F$ and $\boldsymbol{v}_j^F$. The static fine-level graph $G^F = (V^F, E^F)$ describes all persistent features in a MD simulation, which include atom types, atom weights and bond types. These persistent features are used to construct a time-invariant node representation that will be later used for CG-bead embedding in our model. Applying the CG model to the fine-level graphs $\{G_t^F\}$ produces the time series of coarse-level graphs $\{G_t^C\}$, where the CG state G_t^C is defined by the tuple $G_t^C = (V_t^C, E_t^C)$. Each node $\boldsymbol{v}_{m,t}^C \in V_t^C$ represents a CG-bead, and each edge $\boldsymbol{e}_{m,n}^C \in E_t^C$ models an interaction between the CG-beads $\boldsymbol{v}_{m,t}^C$ and $\boldsymbol{v}_{n,t}^C$. Since both non-bonded interactions and bonded interactions at the coarse level are significant for dynamics modeling, the edge set E_t^C contains both CG level bonds and radius cut-off edges constructed from the CG-bead coordinates at time t.

Learning CG-bead type embeddings with Embedding GNN. Each node in the static fine-level graph $\boldsymbol{v}_i^F = [\boldsymbol{a}_i^F, w_i^F]$ is represented with (1) a learnable type embedding $\boldsymbol{a}_i^F$ that is fixed for a given atomic number and (2) a scalar weight w_i^F of the particle. The edge embedding is the sum of the type embedding of the two endpoints and a learnable bond type embedding: $\boldsymbol{e}_{i,j}^F = [\boldsymbol{a}_i^F + \boldsymbol{a}_j^F + \boldsymbol{a}_{i,j}^F]$. The bond type embedding $\boldsymbol{a}_{i,j}^F$ is also fixed for a given bond type. We input this graph G^F to the Embedding GNN GN_E that outputs node embeddings $\boldsymbol{v}_i^F = [\boldsymbol{c}_i^F]$, for all $\boldsymbol{v}_i^F \in V^F$. This learned node embedding contains no positional information and will be used in the next coarse-graining step for representing CG-bead types. The Embedding GNN is trained end-to-end with Dynamics GNN and Score GNN.

Graph-clustering CG model. Our CG model assigns atoms to different atom groups using a graph clustering algorithm (e.g. METIS [39]) over the fine-level graph. The METIS clustering algorithm partitions atoms into groups of roughly equal sizes, while minimizing the number of chemical bonds between atoms in different groups. Each node in the fine-level graph is

[1] If the ground truth MD simulation already uses a CG model, each node will correspond to a CG-bead defined by the CG model, and correspondingly the set of edges will be the set of all CG chemical bonds. For the ease of presentation, in the rest of this paper, we refer to particles in the fine-level graph as "atoms".

assigned a group number: $C(\boldsymbol{v}_{i,t}^F) \in \{1, \dots, M\}$, for all $\boldsymbol{v}_{i,t}^F \in V_t^F$. Here M is the number of atom groups (CG-beads).

Construct CG graph states. We represent each fine-level node $\boldsymbol{v}_{i,t}^F \in V_t^F$ with $\boldsymbol{v}_{i,t}^F = [\boldsymbol{c}_i^F, w_i^F, \boldsymbol{x}_{i,t}^F]$, where $\boldsymbol{c}_i^F$ is the learned node type embedding from GN_E, w_i^F is the weight, and $\boldsymbol{x}_{i,t}^F$ is the position. We can then obtain the coarse-level graph $G_t^C = (V_t^C, E_t^C)$ through grouping atoms in the same group into a CG-bead. Denote the set of fine-level atoms with group number m as $C_m = \{i : C(\boldsymbol{v}_{i,t}^F) = m\}$. The representation of the CG-bead $\boldsymbol{v}_{m,t}^C = [\boldsymbol{c}_m^C, w_m^C, \boldsymbol{x}_{m,t}^C]$ is defined as following:

$$\begin{aligned}
\boldsymbol{c}_m^C &= \underset{C_m}{\mathtt{mean}}(\boldsymbol{c}_i^F) \equiv \frac{\sum_{i \in C_m} \boldsymbol{c}_i^F}{|C_m|} \\
w_m^C &= \underset{C_m}{\mathtt{sum}}(w_i^F) \equiv \sum_{i \in C_m} w_i^F \\
\boldsymbol{x}_{m,t}^C &= \underset{C_m}{\mathtt{CoM}}(\boldsymbol{q}_{i,t}^F, w_i^F) \equiv \frac{\sum_{i \in C_m} w_i^F \boldsymbol{x}_{i,t}^F}{\sum_{i \in C_m} w_i^F}
\end{aligned} \tag{1}$$

The operators $\mathtt{mean}_{C_m}$ stands for taking the mean over C_m, $\mathtt{sum}_{C_m}$ stands for taking the sum over C_m, and $\mathtt{CoM}_{C_m}$ stands for taking the center of mass over C_m. Applying this grouping procedure for all atom groups $m \in \{1, \dots, M\}$ creates the set of all CG nodes $V_t^C = \{\boldsymbol{v}_{m,t}^C : m \in \{1, \dots, M\}\}$ for the coarse-level graph $G_t^C = (V_t^C, E_t^C)$.

We next construct the edges E_t^C. *CG-bonds* are created for bonded atoms separated in different groups. We create a CG-bond $e_{m,n,t}^C$ if there exists a chemical bond between a pair of atoms in group C_m and group C_n. That is:

$$\begin{aligned}
e_{m,n,t}^C \in E_t^C \iff \exists i \in C_m, j \in C_n, \\
\text{such that } e_{i,j}^F \in E^F
\end{aligned} \tag{2}$$

We further create radius cut-off edges by, for each CG-bead, finding all neighboring beads within a pre-defined connectivity raidus r (with consideration to the simulation setup, e.g., periodic boundaries):

$$e_{m,n,t}^C \in E_t^C \iff \|\boldsymbol{x}_{m,t}^C - \boldsymbol{x}_{n,t}^C\| < r \tag{3}$$

We set a large enough connectivity radius to capture significant interactions between all pairs of CG-beads.

Learning CG MD with Dynamics GNN. The Dynamics GNN GN_D inputs a featurized coarse graph state $\phi(\{G_{t-i\Delta t}^C\}_{i=0}^k)$ and outputs a distribution of the time-averaged acceleration for each CG-bead. The input node features $\boldsymbol{v}_{m,t}^C = [\boldsymbol{c}_m^C, w_m^C, \{\dot{\boldsymbol{x}}_{m,t-i\Delta t}^C\}_{i=0}^{k-1}]$ include the CG-bead type embedding $\boldsymbol{c}_m^C$, weight w_m^C, current and k-step history velocities $\{\dot{\boldsymbol{x}}_{m,t-i\Delta t}^C\}_{i=0}^{k-1}$. The input edge features $e_{m,n,t}^C = [\boldsymbol{x}_{m,t}^C - \boldsymbol{x}_{n,t}^C, \|\boldsymbol{x}_{m,t}^C - \boldsymbol{x}_{n,t}^C\|, \boldsymbol{c}_{m,n}^C]$ include displacement and distance between the two end points, and an embedding vector $\boldsymbol{c}_{m,n}^C$ indicating whether $e_{m,n,t}^C$ is a CG-bond or is constructed through radius cut-off. The output is a 3-dimensional Gaussian: $\mathrm{GN}_D(\phi(\{G_{t-i\Delta t}^C\}_{i=0}^k)) = \mathcal{N}(\boldsymbol{\mu}_t, \boldsymbol{\sigma}_t^2) = \{\mathcal{N}(\boldsymbol{\mu}_{m,t}, \boldsymbol{\sigma}_{m,t}^2) : \boldsymbol{v}_{m,t}^C \in V_t^C\}$ [2], where $\boldsymbol{\mu}_t$ and $\boldsymbol{\sigma}_t^2$ are the predicted mean and variance at time t, respectively. The training loss L_{dyn} for predicting the forward dynamics is thus the negative log-likelihood of the ground truth acceleration:

$$L_{\text{dyn}} = -\log \mathcal{N}(\ddot{\boldsymbol{x}}_t^C | \boldsymbol{\mu}_t, \boldsymbol{\sigma}_t^2) \tag{4}$$

The end-to-end training minimizes L_{dyn}, which is only based on single-step prediction of time-integrated acceleration. At inference time (for long simulation), the predicted acceleration $\hat{\ddot{\boldsymbol{x}}}_t \sim \mathcal{N}(\boldsymbol{\mu}_t, \boldsymbol{\sigma}_t^2)$ is sampled from the predicted Gaussian and integrated with a semi-implicit Euler integration to update the positions to the predicted positions $\hat{\boldsymbol{x}}_{t+\Delta t}$:

$$\begin{aligned}
\hat{\dot{\boldsymbol{x}}}_{t+\Delta t} &= \dot{\boldsymbol{x}}_t + \hat{\ddot{\boldsymbol{x}}}_t \Delta t \\
\hat{\boldsymbol{x}}_{t+\Delta t} &= \boldsymbol{x}_t + \hat{\dot{\boldsymbol{x}}}_{t+\Delta t} \Delta t
\end{aligned} \tag{5}$$

Learning to refine CGMD predictions with Score GNN. We introduce the Score GNN, a score-based generative model [38] to resolve the stability issue of long simulation for complex systems. Following the noise conditional score network (NCSN) framework [38, 62], the Score GNN is trained to output the gradients of the history-conditional log density (i.e., scores) given history state information and CG-bead coordinates as input. An incorrect 3D configuration can be refined by iteratively applying the learned scores.

[2] for ease of notation, in the rest of this paper we omit the node/edge indices when referring to every node/edge in the graph

With the refinement step, each forward simulation step follows a predict-then-refine procedure. The Dynamics GNN first predicts the (potentially erroneous) next-step positions, which the Score GNN refines to the final prediction $\hat{\boldsymbol{x}}_{t+\Delta t}$.

During training, the Score GNN is trained to denoise noisy CG-bead positions to the correct positions. Let the noise levels be a sequence of positive scalars $\sigma_1, \ldots, \sigma_L$ satisfying $\sigma_1/\sigma_2 = \cdots = \sigma_{L-1}/\sigma_L > 1$. The noisy positions $\tilde{\boldsymbol{x}}^C_{t+\Delta t}$ is obtained by perturbing the ground truth positions with Gaussian noise: $\tilde{\boldsymbol{x}}^C_{t+\Delta t} = \boldsymbol{x}^C_{t+\Delta t} + \mathcal{N}(0, \sigma^2)$, where multiple levels of noise $\sigma \in \{\sigma_i\}_{i=1}^L$ are used. Due to coarse-graining, the coarse-level dynamics is non-Markovian [37]. Given the current state and historical information $\mathcal{H}$ that causes $\boldsymbol{x}^C_{t+\Delta t}$, the noisy positions follow the distribution with density:

$$p_\sigma(\tilde{\boldsymbol{x}}^C_{t+\Delta t}|\mathcal{H}) = \int p_{\text{data}}(\boldsymbol{x}^C_{t+\Delta t}|\mathcal{H}) \mathcal{N}(\tilde{\boldsymbol{x}}^C_{t+\Delta t}|\boldsymbol{x}^C_{t+\Delta t}, \sigma^2 I) d\boldsymbol{x}^C_{t+\Delta t}$$

The Score GNN outputs the gradients of the log density of particle coordinates that denoise the noisy particle positions $\tilde{\boldsymbol{x}}^C_{t+\Delta t}$ to the ground truth positions $\boldsymbol{x}^C_{t+\Delta t}$, conditional on the current state and historical information. That is: $\forall \sigma \in \{\sigma_i\}_{i=1}^L$,

$$\begin{aligned}
&\text{GN}_S([\boldsymbol{v}^{Ch}_t, \tilde{\boldsymbol{x}}^C_{t+\Delta t}]) \\
&\quad = \nabla_{\tilde{\boldsymbol{x}}^C_{t+\Delta t}} \log p_\sigma(\tilde{\boldsymbol{x}}^C_{t+\Delta t}|\boldsymbol{v}^{Ch}_t)/\sigma \\
&\quad \approx \nabla_{\tilde{\boldsymbol{x}}^C_{t+\Delta t}} \log p_\sigma(\tilde{\boldsymbol{x}}^C_{t+\Delta t}|\mathcal{H})/\sigma \qquad (*) \\
&\quad = \mathbb{E}_{p(\boldsymbol{x}^C_{t+\Delta t}|\mathcal{H})}[(\boldsymbol{x}^C_{t+\Delta t} - \tilde{\boldsymbol{x}}^C_{t+\Delta t})/\sigma^2]
\end{aligned}$$

Note that in step $(*)$ we are approximating $\mathcal{H}$ with learned latent node embeddings $\boldsymbol{v}^{Ch}_t$, which is the last-layer hidden representation output by the Dynamics GNN. $\boldsymbol{v}^{Ch}_t$ contains current state and historical information. The training loss for GN_S is presented in Eq. (6), where $\lambda(\sigma_i) = \sigma_i^2$ is a weighting coefficient that balance the losses at different noise levels. During training, the first expectation in Eq. (6) is obtained by sampling training data from the empirical distribution, and the second expectation is obtained by sampling the Gaussian noise at different levels.

With the Score GNN, training is still end-to-end by jointly optimizing the dynamics loss and score loss: $L = L_{\text{dyn}} + L_{\text{score}}$. At inference time, the refinement starts from the predicted positions from Dynamics GNN. We use annealed Langevin dynamics, which is commonly used in previous work [38], to iteratively apply the learned scores to gradually refine the particle positions, with a decreasing noise term. The predict-then-refine procedure can be repeated to simulate complex systems for long time horizons stably.

$$L_{\text{score}} = \frac{1}{2L} \sum_{i=1}^{L} \lambda(\sigma_i) \mathbb{E}_{\text{data}(\boldsymbol{x}^C_{t+\Delta t}|\mathcal{H})} \mathbb{E}_{p_{\sigma_i}(\tilde{\boldsymbol{x}}^C_{t+\Delta t}|\boldsymbol{x}^C_{t+\Delta t})} \left[\left\| \frac{\text{GN}_S([\boldsymbol{v}^{Ch}_t, \tilde{\boldsymbol{x}}^C_{t+\Delta t}])}{\sigma_i} - \frac{\boldsymbol{x}^C_{t+\Delta t} - \tilde{\boldsymbol{x}}^C_{t+\Delta t}}{\sigma_i^2} \right\|_2^2 \right] \qquad (6)$$

Single-chain CG polymer dataset. The single-chain polymers are simulated using LAMMPS [63], with the force-field parameters and chemical space defined in [43]. All simulations are done in reduced units with characteristic quantities σ for distance and τ for time. Single-chain CG polymer dynamics in implicit solvent evolves according to the Langevin equation using the velocity-Verlet integration scheme. We use a time step of 0.01τ. Training trajectories are 50k τ after removing the initial trajectory for relaxation, and are recorded every 5 τ. Testing trajectories are 5M τ, and are recorded every 500 τ. The polymer interaction is described by the summation of bonded and non-bonded potential energy functions. We refer interested readers to [43] for more details on the simulation setup.

Calculation of single-chain polymer properties. Our main property of study, squared radius of gyration (R_g^2) is computed by:

$$R_g^2 = \left(\frac{\sum_{i \in V} m_i d_i^2}{\sum_{i \in V} m_i} \right)$$

where V is the set of all nodes, m_i is the mass of particle i, and d_i is the distance from particle i to the center of mass.

The relaxation time for R_g^2 is derived from the autocorrelation function (ACF), which is computed as:

$$\mathrm{ACF}(y) = \frac{\langle R_g^2(t)^2 R_g^2(t+y)^2 \rangle_t - (\langle R_g^2(t)^2 \rangle_t)^2}{\langle R_g^2(t)^4 \rangle_t - (\langle R_g^2(t)^2 \rangle_t)^2}$$

Here $\langle \cdot \rangle_t$ stands for averaging over the entire trajectory. The relaxation time $t_{R_g^2}$ is computed by fitting an exponential function $f(y) = \exp(-t_{R_g^2} y)$ to the ACF, and the relaxation time is the time when the ACF decays to $1/e$. It is a highly dynamical long-time property decided by the polymer structure.

Single-chain polymer baseline models. We conduct experiments with two supervised learning baseline models. The first one is a GNN model that takes the polymer chemical graph as input and outputs the mean and standard deviation of R_g^2. Each node in the polymer graph is a CG-bead and each edge is a chemical bond. The GNN uses the Encoder-Processor-Decoder with 10 message-passing layers to process the polymer graph to a latent graph with node/edge embeddings. The MLPs in the GNNs has 2 hiden layers with size 128. The node embeddings are then summed to get the graph embedding, which is then processed by a 2-layer MLP with hidden size 256 to obtain the final prediction of mean and standard deviation of polymer R_g^2. The second LSTM baseline model takes the 1D polymer chain structure as its input, and replaces the GNN encoder with an 2-layer LSTM encoder with hidden size 256. All activation functions in the neural networks are ReLU. The baseline models are optimized with an Adam optimizer with a learning rate of 10^{-3}, exponentially decayed to 5×10^{-4} over 1500 training epochs. Due to the limited time horizon of training data, the baseline models can only fit to high-variance labels, leading to underperforming prediction results.

SPE dataset. The SPE systems are simulated using LAMMPS [63] with the force-field parameters and chemical space defined in [49]. For all systems, there are 50 Li-ions and TFSI-ions in the simulation box, and each polymer chain has 150 atoms in the backbone. The training trajectories are 5-ns long after removing initial equilibration, while the testing trajectories are 50-ns long. Each system is run in the canonical ensemble (nVT) at a temperature of 353K using a multi-timescale integrator with an outer time step of 2 fs for nonbonded interactions, and an inner timestep of 0.5 fs. Both training and testing trajectories are recorded every 2 ps. The atomic interactions are described by the polymer consistent force-field (PCFF+) [64, 65]. We refer interested readers to [49] for more details on the simulation setup.

Calculation of SPE properties. The radial distribution function (RDF) describes the particle density as a function of distance from a reference particle. For a system with many distinct types of particles, we can compute RDF for particular types by counting the neighbor atoms of certain types at various radii and each time step, and average over the entire trajectory. The RDF for particle types A, B at distance r is computed as:

$$\mathrm{RDF}_{A,B}(r) = \frac{d[n_{A,B}(r)]}{4\pi r^2 dr}$$

Here $n_{A,B}(r)$ is the number of particle pairs with types A and B and distance in $[r, r+dr)$, where dr is a small bin size.

Ion transport properties of SPEs are the topic of study for many previous research, and require long-time simulation to estimate. In particular, our experiments focus on particle diffusivity. With a trajectory of time horizon T, the diffusivity D of a particle is computed by:

$$D = \frac{\|\boldsymbol{x}_T - \boldsymbol{x}_0\|_2^2}{6T}$$

where $\boldsymbol{x}_T$ is the position at time T, and $\boldsymbol{x}_0$ is the position at time 0. The diffusivity of a type of particle (e.g., Li-ion) is then computed by averaging the particle diffusivity over all particles of that type.

SPE diffusivity prediction baseline model. We adopt the GNN model proposed in [49] and refer interested readers to [49] for more details. The only modification we make is changing the training objective, so as to rectify the overestimation coming from short MD horizon of the training data. We let the baseline model fit the 5 ns diffusivity curves (curves in Fig. 5 a) by predicting two parameters in the function: $f(t) = y + e^{-\theta t}$. Therefore, the model approximates the converging process of diffusivity with exponential decay. During evaluation, we set

$t = 50$ ns to obtain the model prediction for 50-ns diffusivity. However, without any long training trajectories, it is very challenging to guess the decaying process of diffusivity for various SPEs. The baseline model performs better than using 5-ns ground truth MD, but still significantly overestimates particle diffusivity.

Data Availbility

We generate the single-chain polymer dataset used in this paper with the simulation protocol of [43]. This dataset is available at https://zenodo.org/record/6764836#.YrqP9-xKjzc. The SPE dataset used in this paper is adopted from [49], and can be requested from the original authors.

Code Availbility

We implement our model primarily using PyTorch [66] and PyTorch Geometric [67]. Our code is open-sourced at https://github.com/kyonofx/mlcgmd.

Acknowledgments

We pay tribute to Octavian-Eugen Ganea (1987-2022), dear colleague and friend who we had many inspiring discussions over this work. We thank Wujie Wang, Tzyy-Shyang Lin, Gabriele Corso, Bowen Jing, Shangyuan Tong, Yilun Xu, Hannes Stärk and the rest of the TJ group members for their helpful comments and suggestions. We thank Michael A. Webb for his advice and support on the single-chain coarse-grained polymer dataset. We gratefully thank the Community Resource for Innovation in Polymer Technology, a project supported by the National Science Foundation (NSF) Convergence Accelerator program (Convergence Accelerator Research 2134795), and MIT-GIST collaboration for support. The authors also acknowledge the MIT SuperCloud and the Lincoln Laboratory Supercomputing Center for providing HPC resources.

References

[1] Webb, M.A., Jung, Y., Pesko, D.M., Savoie, B.M., Yamamoto, U., Coates, G.W., Balsara, N.P., Wang, Z.-G., Miller III, T.F.: Systematic computational and experimental investigation of lithium-ion transport mechanisms in polyester-based polymer electrolytes. ACS central science **1**(4), 198–205 (2015)

[2] Molinari, N., Mailoa, J.P., Kozinsky, B.: Effect of salt concentration on ion clustering and transport in polymer solid electrolytes: a molecular dynamics study of peo–litfsi. Chemistry of Materials **30**(18), 6298–6306 (2018)

[3] Wang, Y., Xie, T., France-Lanord, A., Berkley, A., Johnson, J.A., Shao-Horn, Y., Grossman, J.C.: Toward designing highly conductive polymer electrolytes by machine learning assisted coarse-grained molecular dynamics. Chemistry of Materials **32**(10), 4144–4151 (2020)

[4] Lindorff-Larsen, K., Piana, S., Dror, R.O., Shaw, D.E.: How fast-folding proteins fold. Science **334**(6055), 517–520 (2011)

[5] Karplus, M., Kuriyan, J.: Molecular dynamics and protein function. Proceedings of the National Academy of Sciences **102**(19), 6679–6685 (2005)

[6] Schoenholz, S., Cubuk, E.D.: Jax md: a framework for differentiable physics. Advances in Neural Information Processing Systems **33** (2020)

[7] Doerr, S., Majewski, M., Pérez, A., Krämer, A., Clementi, C., Noe, F., Giorgino, T., De Fabritiis, G.: Torchmd: A deep learning framework for molecular simulations. Journal of Chemical Theory and Computation **17**(4), 2355–2363 (2021)

[8] Noé, F., Tkatchenko, A., Müller, K.-R., Clementi, C.: Machine learning for molecular simulation. Annual review of physical chemistry **71**, 361–390 (2020)

[9] Unke, O.T., Chmiela, S., Sauceda, H.E., Gastegger, M., Poltavsky, I., Sch utt, K.T., Tkatchenko, A., Müller, K.-R.: Machine learning force fields. Chemical Reviews **121**(16), 10142–10186 (2021)

[10] Friederich, P., Häse, F., Proppe, J., Aspuru-Guzik, A.: Machine-learned potentials for next-generation matter simulations. Nature Materials **20**(6), 750–761 (2021)

[11] Li, Z., Meidani, K., Yadav, P., Barati Farimani, A.: Graph neural networks accelerated molecular dynamics. The Journal of Chemical Physics **156**(14), 144103 (2022)

[12] Chmiela, S., Tkatchenko, A., Sauceda, H.E., Poltavsky, I., Schütt, K.T., Müller, K.-R.: Machine learning of accurate energy-conserving molecular force fields. Science Advances **3**(5), 1603015 (2017)

[13] Chmiela, S., Sauceda, H.E., Müller, K.-R., Tkatchenko, A.: Towards exact molecular dynamics simulations with machine-learned force fields. Nature communications **9**(1), 1–10 (2018)

[14] Zhang, L., Han, J., Wang, H., Car, R., E, W.: Deep potential molecular dynamics: A scalable model with the accuracy of quantum mechanics. Phys. Rev. Lett. **120**, 143001 (2018)

[15] Jia, W., Wang, H., Chen, M., Lu, D., Lin, L., Car, R., Weinan, E., Zhang, L.: Pushing the limit of molecular dynamics with ab initio accuracy to 100 million atoms with machine learning. In: SC20: International Conference for High Performance Computing, Networking, Storage and Analysis, pp. 1–14 (2020). IEEE

[16] Unke, O.T., Chmiela, S., Gastegger, M., Schütt, K.T., Sauceda, H.E., Müller, K.-R.: Spookynet: Learning force fields with electronic degrees of freedom and nonlocal effects. Nature communications **12**(1), 1–14 (2021)

[17] Park, C.W., Kornbluth, M., Vandermause, J., Wolverton, C., Kozinsky, B., Mailoa, J.P.: Accurate and scalable graph neural network force field and molecular dynamics with direct force architecture. npj Computational Materials **7**(1), 1–9 (2021)

[18] Stocker, S., Gasteiger, J., Becker, F., Günnemann, S., Margraf, J.: How robust are modern graph neural network potentials in long and hot molecular dynamics simulations? (2022)

[19] Wang, W., Gómez-Bombarelli, R.: Coarse-graining auto-encoders for molecular dynamics. npj Computational Materials **5**(1), 125 (2019)

[20] Wang, J., Olsson, S., Wehmeyer, C., Pérez, A., Charron, N.E., De Fabritiis, G., Noé, F., Clementi, C.: Machine learning of coarse-grained molecular dynamics force fields. ACS central science **5**(5), 755–767 (2019)

[21] Husic, B.E., Charron, N.E., Lemm, D., Wang, J., Pérez, A., Majewski, M., Krämer, A., Chen, Y., Olsson, S., de Fabritiis, G., *et al.*: Coarse graining molecular dynamics with graph neural networks. The Journal of chemical physics **153**(19), 194101 (2020)

[22] Noid, W.G.: Perspective: Coarse-grained models for biomolecular systems. The Journal of chemical physics **139**(9), 09–2011 (2013)

[23] Bernardi, R.C., Melo, M.C.R., Schulten, K.: Enhanced sampling techniques in molecular dynamics simulations of biological systems. Biochimica et Biophysica Acta (BBA) - General Subjects **1850**(5), 872–877 (2015)

[24] Yang, Y.I., Shao, Q., Zhang, J., Yang, L., Gao, Y.Q.: Enhanced sampling in molecular dynamics. The Journal of chemical physics **151**(7), 070902 (2019)

[25] Wang, D., Wang, Y., Chang, J., Zhang, L., Wang, H., E., W.: Efficient sampling of high-dimensional free energy landscapes using adaptive reinforced dynamics. Nature Computational Science (2021)

[26] Cendagorta, J.R., Tolpin, J., Schneider, E., Topper, R.Q., Tuckerman, M.E.: Comparison of the performance of machine learning models in representing high-dimensional free energy surfaces and generating observables. The Journal of Physical Chemistry B **124**(18), 3647–3660 (2020)

[27] Schneider, E., Dai, L., Topper, R.Q., Drechsel-Grau, C., Tuckerman, M.E.: Stochastic neural network approach for learning high-dimensional free energy surfaces. Phys. Rev. Lett. **119**, 150601 (2017). https://doi.org/10.1103/PhysRevLett.119.150601

[28] Sultan, M.M., Wayment-Steele, H.K., Pande, V.S.: Transferable neural networks for enhanced sampling of protein dynamics. Journal of chemical theory and computation **14**(4), 1887–1894 (2018)

[29] Laio, A., Rodriguez-Fortea, A., Gervasio, F.L., Ceccarelli, M., Parrinello, M.: Assessing the accuracy of metadynamics. The journal of physical chemistry B **109**(14), 6714–6721 (2005)

[30] Stelzl, L.S., Hummer, G.: Kinetics from replica exchange molecular dynamics simulations. Journal of chemical theory and computation **13**(8), 3927–3935 (2017)

[31] Noé, F., Olsson, S., Köhler, J., Wu, H.: Boltzmann generators: Sampling equilibrium states of many-body systems with deep learning. Science **365**(6457) (2019)

[32] Mahmoud, A.H., Masters, M., Lee, S.J., Lill, M.A.: Accurate sampling of macromolecular conformations using adaptive deep learning and coarse-grained representation. Journal of Chemical Information and Modeling (2022)

[33] Li, Y., Wu, J., Zhu, J.-Y., Tenenbaum, J.B., Torralba, A., Tedrake, R.: Propagation networks for model-based control under partial observation. In: ICRA (2019)

[34] Li, Y., Wu, J., Tedrake, R., Tenenbaum, J.B., Torralba, A.: Learning particle dynamics for manipulating rigid bodies, deformable objects, and fluids. In: ICLR (2019)

[35] Sanchez-Gonzalez, A., Godwin, J., Pfaff, T., Ying, R., Leskovec, J., Battaglia, P.: Learning to simulate complex physics with graph networks. In: International Conference on Machine Learning, pp. 8459–8468 (2020). PMLR

[36] Pfaff, T., Fortunato, M., Sanchez-Gonzalez, A., Battaglia, P.W.: Learning mesh-based simulation with graph networks. In: International Conference on Learning Representations (2021)

[37] Klippenstein, V., Tripathy, M., Jung, G., Schmid, F., van der Vegt, N.F.: Introducing memory in coarse-grained molecular simulations. The Journal of Physical Chemistry B **125**(19), 4931–4954 (2021)

[38] Song, Y., Ermon, S.: Generative modeling by estimating gradients of the data distribution. In: Wallach, H.M., Larochelle, H., Beygelzimer, A., d'Alché-Buc, F., Fox, E.B., Garnett, R. (eds.) Advances in Neural Information Processing Systems 32: Annual Conference on Neural Information Processing Systems 2019, NeurIPS 2019, December 8-14, 2019, Vancouver, BC, Canada, pp. 11895–11907 (2019)

[39] Karypis, G., Kumar, V.: A fast and high quality multilevel scheme for partitioning irregular graphs. SIAM Journal on scientific Computing **20**(1), 359–392 (1998)

[40] Marrink, S.J., Risselada, H.J., Yefimov, S., Tieleman, D.P., De Vries, A.H.: The martini force field: coarse grained model for biomolecular simulations. The journal of physical chemistry B **111**(27), 7812–7824 (2007)

[41] de Pablo, J.J.: Coarse-grained simulations of macromolecules: from dna to nanocomposites. Annual review of physical chemistry **62**, 555–574 (2011)

[42] Shmilovich, K., Mansbach, R.A., Sidky, H., Dunne, O.E., Panda, S.S., Tovar, J.D., Ferguson, A.L.: Discovery of self-assembling π-conjugated peptides by active learning-directed coarse-grained molecular simulation. The Journal of Physical Chemistry B **124**(19), 3873–3891 (2020)

[43] Webb, M.A., Jackson, N.E., Gil, P.S., de Pablo, J.J.: Targeted sequence design within the coarse-grained polymer genome. Science Advances **6**(43), 6216 (2020)

[44] Altintas, O., Barner-Kowollik, C.: Single-chain folding of synthetic polymers: a critical update. Macromolecular rapid communications **37**(1), 29–46 (2016)

[45] Upadhya, R., Murthy, N.S., Hoop, C.L., Kosuri, S., Nanda, V., Kohn, J., Baum, J., Gormley, A.J.: Pet-raft and saxs: High throughput tools to study compactness and flexibility of single-chain polymer nanoparticles. Macromolecules **52**(21), 8295–8304 (2019)

[46] Hochreiter, S., Schmidhuber, J.: Long short-term memory. Neural computation **9**(8), 1735–1780 (1997)

[47] Zhou, D., Shanmukaraj, D., Tkacheva, A., Armand, M., Wang, G.: Polymer electrolytes for lithium-based batteries: Advances and prospects. Chem **5**(9), 2326–2352 (2019)

[48] Savoie, B.M., Webb, M.A., Miller III, T.F.: Enhancing cation diffusion and suppressing anion diffusion via lewis-acidic polymer electrolytes. The journal of physical chemistry letters **8**(3), 641–646 (2017)

[49] Xie, T., France-Lanord, A., Wang, Y., Lopez, J., Stolberg, M.A., Hill, M., Leverick, G.M., Gomez-Bombarelli, R., Johnson, J.A., Shao-Horn, Y., et al.: Accelerating the screening of amorphous polymer electrolytes by learning to reduce random and systematic errors in molecular dynamics simulations. arXiv preprint arXiv:2101.05339 (2021)

[50] Thomas, N., Smidt, T., Kearnes, S., Yang, L., Li, L., Kohlhoff, K., Riley, P.: Tensor field networks: Rotation-and translation-equivariant neural networks for 3d point clouds. arXiv preprint arXiv:1802.08219 (2018)

[51] Satorras, V.G., Hoogeboom, E., Welling, M.: E(n) equivariant graph neural networks. In: Meila, M., Zhang, T. (eds.) Proceedings of the 38th International Conference on Machine Learning. Proceedings of Machine Learning Research, vol. 139, pp. 9323–9332 (2021). PMLR

[52] Batzner, S., Musaelian, A., Sun, L., Geiger, M., Mailoa, J.P., Kornbluth, M., Molinari, N., Smidt, T.E., Kozinsky, B.: Se (3)-equivariant graph neural networks for data-efficient and accurate interatomic potentials. arXiv preprint arXiv:2101.03164 (2021)

[53] Gasteiger, J., Groß, J., Günnemann, S.: Directional message passing for molecular graphs. In: International Conference on Learning Representations (2020)

[54] Gasteiger, J., Becker, F., Günnemann, S.: Gemnet: Universal directional graph neural networks for molecules. In: Beygelzimer, A., Dauphin, Y., Liang, P., Vaughan, J.W. (eds.) Advances in Neural Information Processing Systems (2021)

[55] Kmiecik, S., Gront, D., Kolinski, M., Wieteska, L., Dawid, A.E., Kolinski, A.: Coarse-grained protein models and their applications. Chemical reviews **116**(14), 7898–7936 (2016)

[56] Souza, P.C., Alessandri, R., Barnoud, J., Thallmair, S., Faustino, I., Grünewald, F., Patmanidis, I., Abdizadeh, H., Bruininks, B.M., Wassenaar, T.A., *et al.*: Martini 3: a general purpose force field for coarse-grained molecular dynamics. Nature methods **18**(4), 382–388 (2021)

[57] Zhang, L., Han, J., Wang, H., Car, R., E, W.: Deepcg: Constructing coarse-grained models via deep neural networks. The Journal of chemical physics **149**(3), 034101 (2018)

[58] Li, Z., Wellawatte, G.P., Chakraborty, M., Gandhi, H.A., Xu, C., White, A.D.: Graph neural network based coarse-grained mapping prediction. Chemical science **11**(35), 9524–9531 (2020)

[59] Sadeghi, M., Noé, F.: Large-scale simulation of biomembranes incorporating realistic kinetics into coarse-grained models. Nature communications **11**(1), 1–13 (2020)

[60] Köhler, J., Chen, Y., Krämer, A., Clementi, C., Noé, F.: Force-matching coarse-graining without forces. arXiv preprint

arXiv:2203.11167 (2022)

[61] Wang, W., Xu, M., Cai, C., Miller, B.K., Smidt, T., Wang, Y., Tang, J., Gómez-Bombarelli, R.: Generative coarse-graining of molecular conformations. arXiv preprint arXiv:2201.12176 (2022)

[62] Shi, C., Luo, S., Xu, M., Tang, J.: Learning gradient fields for molecular conformation generation. In: Meila, M., Zhang, T. (eds.) Proceedings of the 38th International Conference on Machine Learning, ICML 2021, 18-24 July 2021, Virtual Event. Proceedings of Machine Learning Research, vol. 139, pp. 9558–9568 (2021). PMLR

[63] Thompson, A.P., Aktulga, H.M., Berger, R., Bolintineanu, D.S., Brown, W.M., Crozier, P.S., in 't Veld, P.J., Kohlmeyer, A., Moore, S.G., Nguyen, T.D., Shan, R., Stevens, M.J., Tranchida, J., Trott, C., Plimpton, S.J.: LAMMPS - a flexible simulation tool for particle-based materials modeling at the atomic, meso, and continuum scales. Comp. Phys. Comm. **271**, 108171 (2022)

[64] Sun, H.: Force field for computation of conformational energies, structures, and vibrational frequencies of aromatic polyesters. Journal of Computational Chemistry **15**(7), 752–768 (1994)

[65] Rigby, D., Sun, H., Eichinger, B.: Computer simulations of poly (ethylene oxide): force field, pvt diagram and cyclization behaviour. Polymer International **44**(3), 311–330 (1997)

[66] Paszke, A., Gross, S., Massa, F., Lerer, A., Bradbury, J., Chanan, G., Killeen, T., Lin, Z., Gimelshein, N., Antiga, L., Desmaison, A., Kopf, A., Yang, E., DeVito, Z., Raison, M., Tejani, A., Chilamkurthy, S., Steiner, B., Fang, L., Bai, J., Chintala, S.: Pytorch: An imperative style, high-performance deep learning library. In: Wallach, H., Larochelle, H., Beygelzimer, A., d' Alché-Buc, F., Fox, E., Garnett, R. (eds.) Advances in Neural Information Processing Systems 32, pp. 8024–8035 (2019). Curran Associates, Inc.

[67] Fey, M., Lenssen, J.E.: Fast graph representation learning with PyTorch Geometric. In: ICLR Workshop on Representation Learning on Graphs and Manifolds (2019)

Supplementary Information

We conduct ablation experiments to study the influence of our modeling choices, using the SPE dataset.

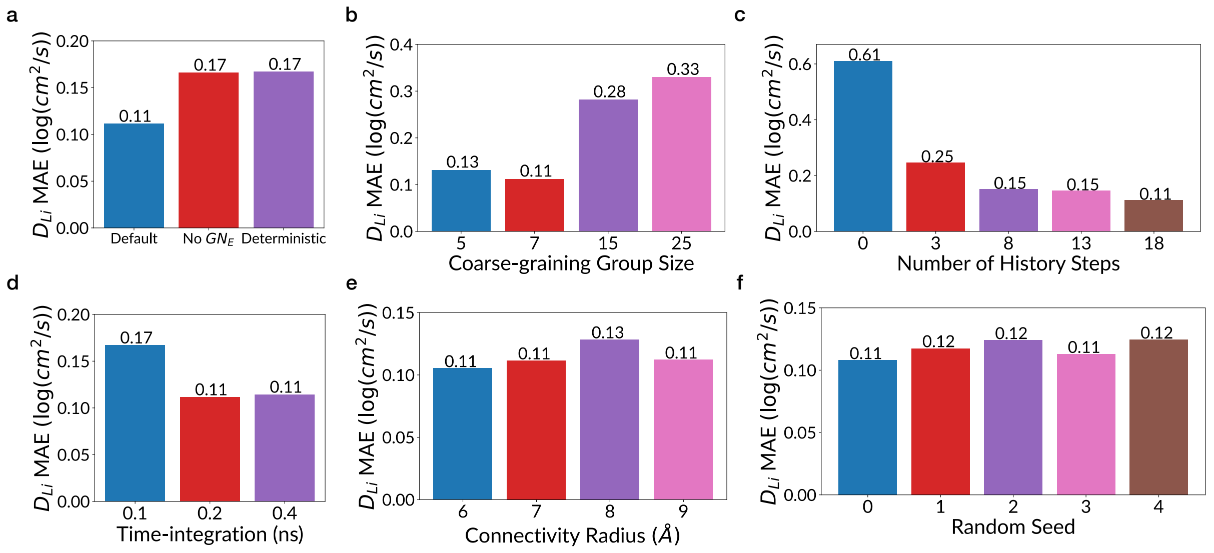

Fig. 6 (a) Comparison of our default model, a model without the Embedding GNN at the fine-level graph, and a model that predicts deterministic acceleration for each particle. (b) Comparison of different coarse-graining atom group sizes. The atom group size is the number of atoms contained in each CG-bead. Performance drops when the coarse-graining is too fine (5) or too coarse(15, 25). (c) Comparison of different history lengths for predicting the dynamics. We observe that longer history helps improve the model performance. (d) Comparison of different time-integration step lengths. A longer time-integration removes high-frequency information and simplifies the dynamics, making it easier to learn. On the other hand, the long-time property of particle diffusivity does not require high-frequency information to estimate accurately. (e) Comparison of different connectivity radii when building the coarse-level graph. A radius of 6 Åis sufficient for modeling the SPE systems. (f) Comparison of different random seeds using the same model. Our model does stochastic rollouts, and the performance is robust to random seeds.

Fine-level Embedding GNN GN_E**.** (Fig. 6 (a)) Our model uses a fine-level embedding GNN to learn CG-bead embedding that enclose local structural information. We can remove this fine-level GNN and let the CG-bead embedding be the mean over the atom type embedding in each atom group. As shown in Fig. 6 (a), model performance significantly drops without the Embedding GNN.

Stochastic dynamics prediction. (Fig. 6 (a)) We attempt to let our model output deterministic acceleration at each forward simulation step. However, the inherent uncertainty makes the model predict very small movement for all particles at every step, and the model performance significantly drops. The small movements lead to slow transport of particles, and causes underestimation of Li-ion diffusivity, as shown in Fig. 7 (a). Such unrealistic dynamics also makes long simulation unstable. This is demonstrated in Fig. 7 (b), which shows that a deterministic model has a higher number of bead collision with an increasing trend through time.

Coarse-graining group size. (Fig. 6 (b)) We experimented with different coarse-graining group size. We observe that in terms of capturing particle diffusivity, using a group size of 7 outperforms finer (5) and coarser (15, 25) coarse-graining. We hypothesize that the finer system is hard to model accurately with limited training data, while the coarser system loses important information for accurate dynamics modeling. This result further suggests the optimal coarse-grained modeling should be conditional on the objective of MD simulation.

Use of historical information for prediction. (Fig. 6 (c)) The spatio-temporal coarse-graining introduces memory effects to the resulting dynamics. Our model uses historical information by utilizing

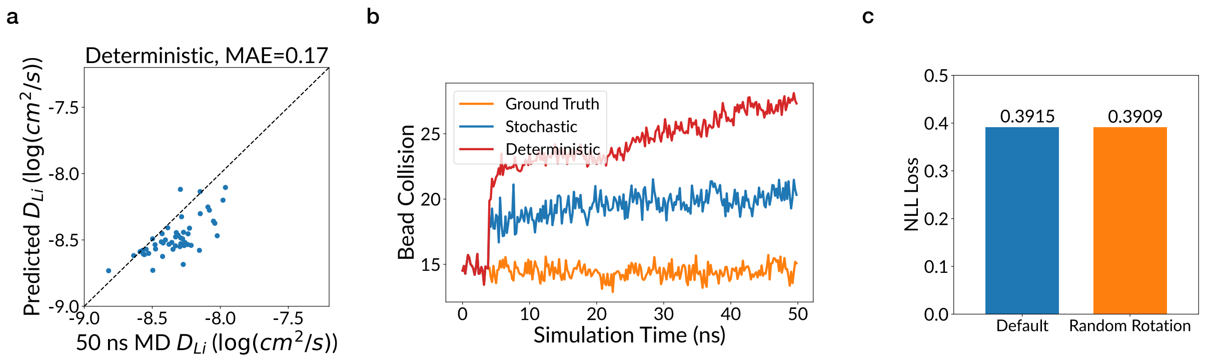

Fig. 7 (a) Li-ion diffusivity estimation performance of the deterministic learned simulator. The model predicts small movements at every step, leading to slower ion transport and underestimation of Li-ion diffusivity. (b) Bead collision as a function of time, averaged over the 50 testing SPEs. the deterministic model's prediction becomes increasingly unphysical as simulation proceeds. (c) The negative log-likelihood (NLL) loss of model prediction on testing polymers. Model performance remains the same when the input structures are randomly rotated before being fed into the model.

k-step historical velocities in dynamics prediction, and we experimented with $k = 0, 3, 8, 13, 18$, under a time-integration of 0.2 ns per step. We observe that longer history as input leads to better performance.

Time-integration step size. (Fig. 6 (d)) We experimented with different time-integration step size. We observe that a longer time-integration gives the best performance. We hypothesize this is due to the dynamics simplification effect of long time-integration, while the loss of high-frequency dynamics does not damage the estimation accuracy of particle diffusivity under long-time simulation.

Connectivity radius. (Fig. 6 (e)) Our coarse-level graphs contain both CG-bonds and radius cut-off edges. The radius cut-off edges model non-bonded interactions. We experimented with radius 6, 7, 8, 9 Å, but found no significant performance difference. We conclude that a radius of 6 Åis sufficient for modeling the SPE non-bonded dynamics.

Random seeds. (Fig. 6 (f)) As our model does stochastic simulation, we examine its robustness against the random seed. We rollout 5 times using the same model and observed no significant performance difference across random seeds.

Rotational equivariance. We verify our learned simulator being rotationally equivariant by applying random rotations at X, Y, and Z axes to input data, and compute the dynamics prediction loss, before and after the random rotations. Fig. 7 (c) shows that the model test time performance is unchanged irrespective of the random rotations. Therefore, our learned simulator is effectively rotational equivariant by learning from data. x

The coarse-graining process. We illustrate the coarse-graining process for the single-chain CG polymers (Fig. 8) and the SPE systems (Fig. 9 (a)). For single-chain polymers, the graph clustering algorithm cuts the chain into segments of roughly equal sizes, and forms a coarse-level chain, capturing the overall shape of the polymer. For SPE systems, atoms belonging to different molecules are never coarse-grained into the same group. So the Li-ions are never coarse-grained, while each TFSI-ion (with 15 atoms) is coarse-grained into two CG-beads. The system complexity is significantly reduced after coarse-graining. At a high level, the graph clustering algorithm groups nearby bonded atoms under the constraint that atom groups should be of similar sizes. Fig. 9 (b,c) show the atom group size distribution for the single-chain polymer dataset (Fig. 9 (b)) and the SPE dataset (Fig. 9 (c)), confirming that the CG-beads are of similar sizes and contain the desired number of atoms.

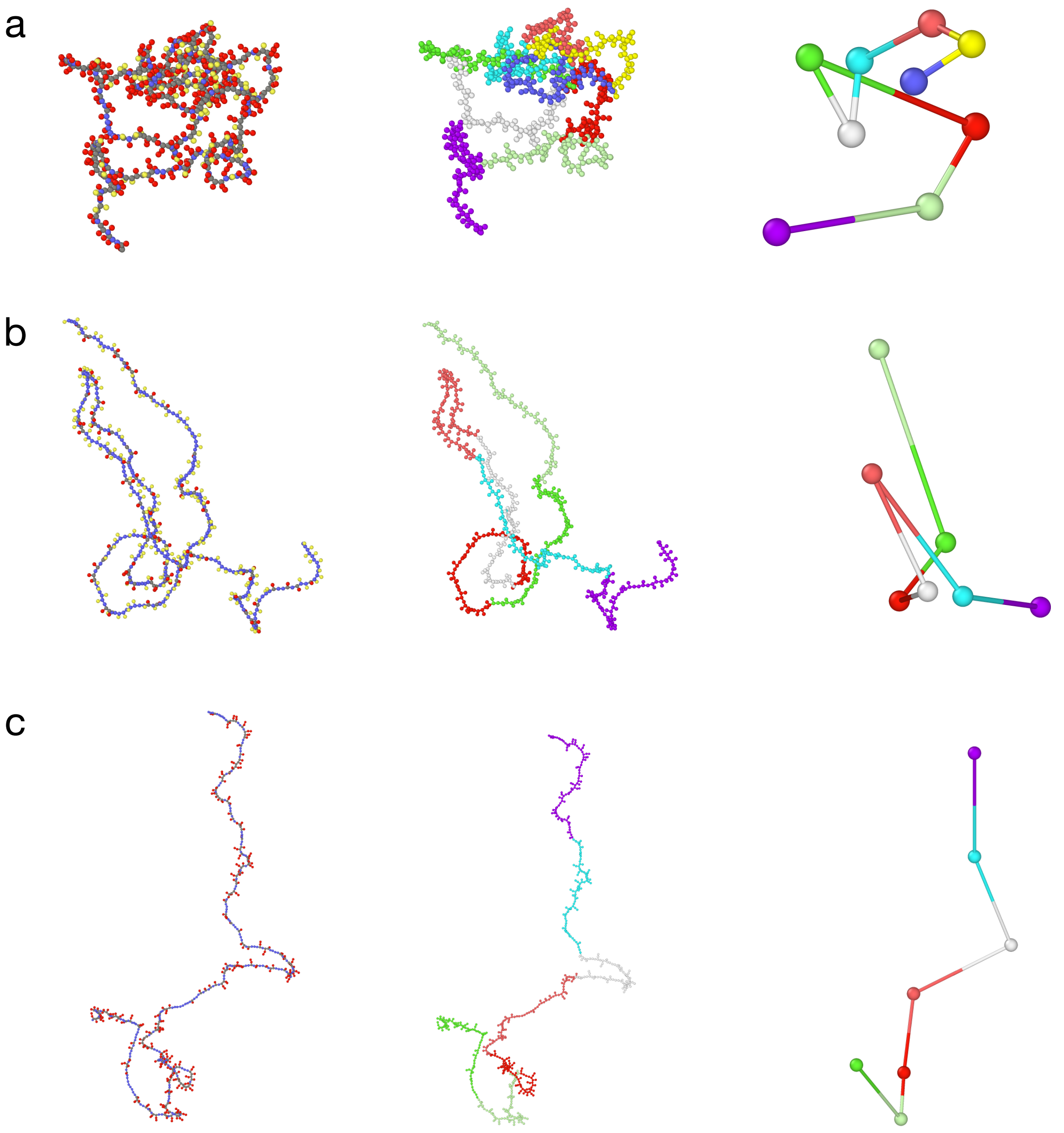

Fig. 8 (a,b,c) The coarse-graining mapping of three example single-chain CG polymers. The first column is the original CG polymer structure with the color indicating the bead type; the second column colors beads according to their assigned super CG-bead; the third column shows the resulting CG system.

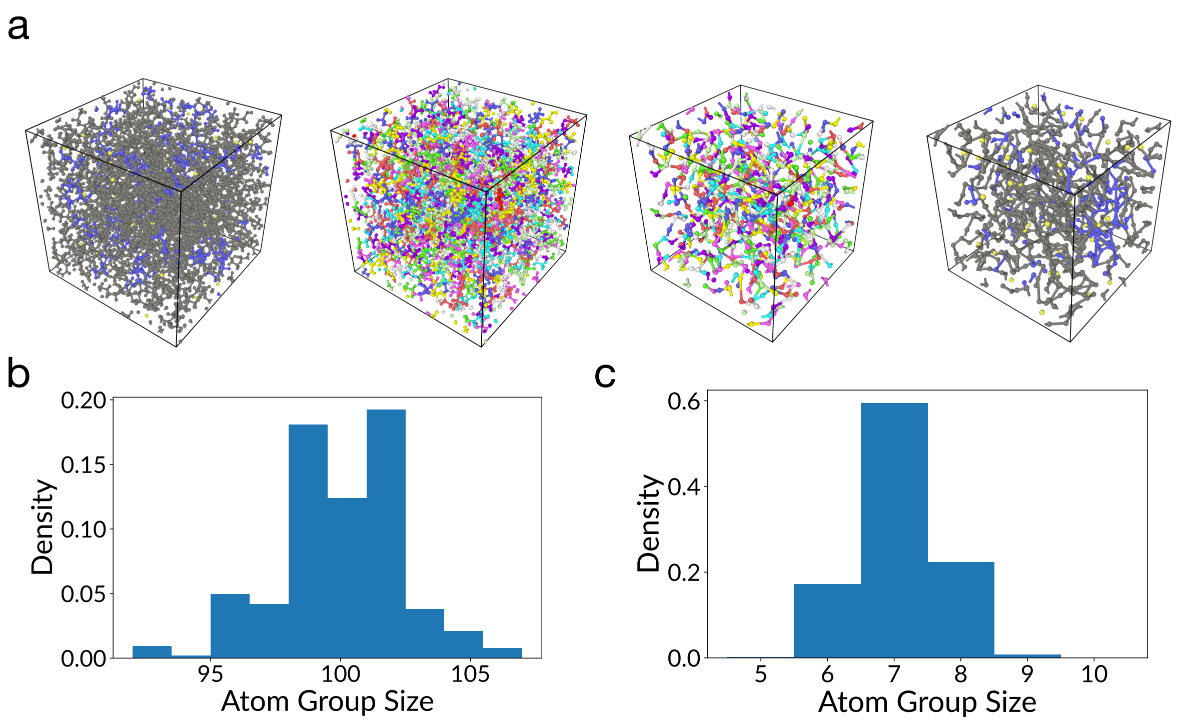

Fig. 9 (a) The coarse-graining mapping an example SPE system. The first column shows the full atomic structure; the second column colors atoms according to their assigned CG-bead; the third column shows the resulting CG system; the fourth column shows the CG structure with color indicating the type of a bead: Li-ion, TFSI-ion or polymer. (b) Distribution of CG-bead atom group sizes for the single-chain CG polymer dataset. The clustering algorithm partitions a polymer into groups of roughly equal sizes of around 100. (c) Distribution of CG-bead atom group sizes for the SPE dataset. The clustering algorithm partitions the atoms into groups of roughly equal sizes of around 7.

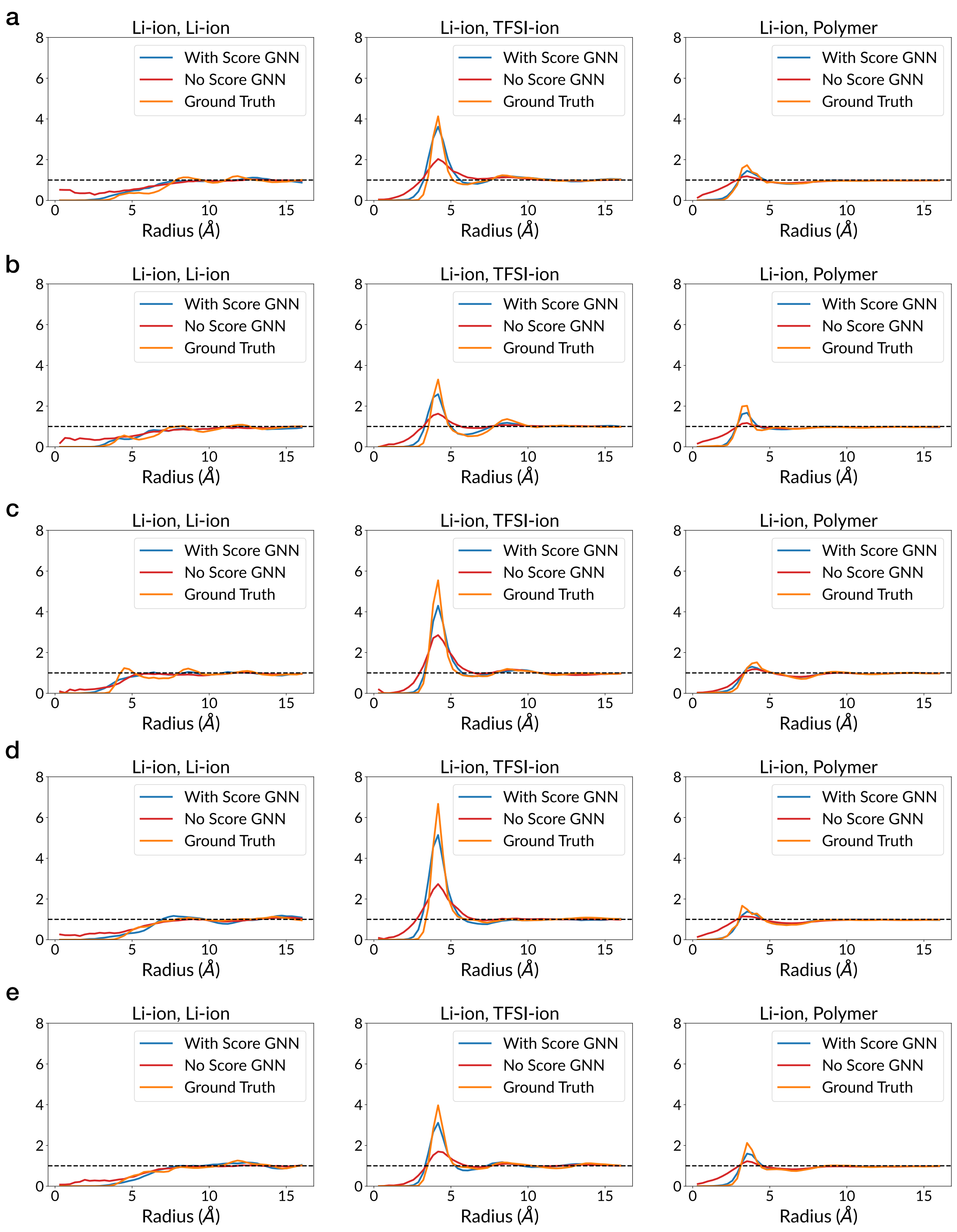

Fig. 10 (a,b,c,d,e) Comparison of our model with/without the Score GNN refinement, and the ground truth MD simulation, on RDF of Li-ions (column 1), RDF of Li-ions and TFSI-ions (column 2), and RDF of Li-ions and polymer particles (column 3) for five sampled SPEs.